Journal of ELECTRONIC MATERIALS, Vol. 49, No. 3, 2020
https://doi.org/10.1007/s11664-019-07498-8

Tailoring of Electromagnetic Absorption in Substituted Hexaferrites from 8.2 GHz to 12.4 GHz

HARSIMRAT KAUR,[1,9] ANUPMA MARWAHA,[1,10] CHARANJEET SINGH ,[2,11,12] SUKHLEEN BINDRA NARANG,[3] RAJSHREE JOTANIA,[4] YANG BAI,[5] SANJAY R. MISHRA,[6] DHARMENDRA SINGH,[7] A.S.B. SOMBRA,[8] MADHAV GHIMIRE,[6] and PREKSHA DHRUV[4]

1.—Department of ECE, Sant Longowal Institute of Engineering and Technology, Longowal, Sangrur, Punjab, India. 2.—Department of ECE, Lovely Professional University, Phagwara, Punjab, India. 3.—Department of Electronics Technology, Guru Nanak Dev University, Amritsar, Punjab, India. 4.—Department of Physics, Electronics and Space Science, University School of Sciences, Gujarat University, Ahmadabad, Gujarat, India. 5.—School of Materials Science and Engineering, University of Science and Technology, Beijing 100083, China. 6.—Department of Physics, University of Memphis, Memphis, TN, USA. 7.—Department of ECE, Indian Institute of Technology Roorkee, Roorkee, India. 8.—Department of Physics, (LOCEM), Federal University of Ceará (UFC), Pici Campus, Fortaleza, Ceara, Brazil. 9.—Department of ECE, CT Institute of Engineering and Management Technology, Jalandhar, Punjab, India. 10.—e-mail: marwaha_anupma@yahoo.co.in. 11.—e-mail: charanjeet2003@rediffmail.com. 12.—e-mail: rcharanjeet@gmail.com

Microwave absorbers are an important topic of interest to mitigate electromagnetic interference. Here, we have investigated electromagnetic absorption properties of $Ba_{0.5}Sr_{0.5}Co_xIn_xFe_{12-2x}O_{19}$ hexaferrite prepared by the conventional ceramic method. M-type hexagonal structure in the compositions was confirmed from x-ray diffraction analysis. The role of Co^{2+} and In^{3+}, thickness of composition and frequency on the electromagnetic absorption in the ferrite compositions has been explored from 8.2 GHz to 12.4 GHz. It was found that both Co^{2+}-In^{3+} increased microwave/electromagnetic absorption with broad bandwidth, decreased the thickness and enhanced impedance matching. The reflection loss of −39.99 dB was noted in the composition $x = 0.2$ for the thickness of 1.6 mm and a frequency of 11.14 GHz. The results conclude that investigated compositions of $Ba_{0.5}Sr_{0.5}Co_xIn_xFe_{12-2x}O_{19}$ ferrite ameliorate absorber applications.

Key words: Ferrites, microwave absorption, quarter-wavelength mechanism, impedance matching

INTRODUCTION

The widespread development and technological applications of high speed electrical/electronic devices have caused enormous electromagnetic pollution in the atmosphere. M-type hexaferrites have been studied in the form of absorbers to mitigate such interference in the microwave band owing to their good chemical and physical properties.[1–4] The absorbers are evaluated in terms of high reflection loss, broad/narrow −10-dB/−20-dB bandwidth and small thickness. The basic idea is to tune the microwave absorption by exploiting the frequency region, impedance as well as thickness of absorber. Researchers have explored microwave-absorbing characteristics of ferrites with divalent, trivalent and tetravalent substitutions and different frequency regimes.[5–13] The absorption in the desired microwave spectrum and its optimization is explored mainly by considering dielectric loss and

(Received April 16, 2019; accepted July 27, 2019; published online August 19, 2019)

magnetic loss. Authors have examined the impedance tuning condition for an ideal absorber as $Z_{in} = 1$, where Z_{in} is the input impedance of absorber. On the contrary, mathematical analysis for absorbance was not explored. The correlation between hysteresis parameters and microwave absorption need to be explored more. Keeping in view of these rebuttals, this paper explores microwave absorption by substitution of Co^{2+}-In^{3+} in $Ba_{0.5}Sr_{0.5}Co_xIn_xFe_{12-2x}O_{19}$ ferrite. The selection of substituted Co^{2+} and In^{3+} is attributed to their large ionic radii and it can cause their occupancy on octahedral sites in order to have a soft ferrite nature required for the absorber. To the author's best knowledge, microwave absorption in the proposed chemical composition has not been investigated yet. The expected contribution of pertinent models behind the variation of absorption has also been discussed.

EXPERIMENTAL PROCEDURE

The conventional ceramic method was used to synthesize hexaferrite compositions of $Ba_{0.5}Sr_{0.5}(CoIn)_xFe_{(12-2x)}O_{19}$ with $x = 0.0$ for unsubstituted ferrite $Ba_{0.5}Sr_{0.5}Fe_{12}O_{19}$ and $x = 0.2$, 0.4, 0.6, 0.8 and 1.0 for substituted ferrite.[14] Analytical reagent (AR) grade (Sigma-Aldrich, 99.98% pure) $BaCO_3$, $SrCO_3$, $CoCO_3$, In_2O_3 and Fe_2O_3 were used as the starting materials. The required powders were mixed thoroughly in an electrically operated pestle-mortar with distilled water for 8 h before pre- and final sintering. The powders were left for drying at room temperature, and thereafter the same were heated at a temperature of 1000°C for 10 h in a software-programmed electric furnace. The sieving of powders was done with 220 B.S.S mesh size of sieves, and pellets were made from the obtained powder with help of a hydraulic press with 75-KN/m^2 uniform pressure. Then, pellets were heated again at a temperature of 1150°C for 15 h.

A Philips X'pert diffractometer was used to check the structure characterization through x-ray diffraction (XRD) technique. The rectangularly shaped compositions were placed in the rectangular waveguide, and the waveguide was coupled with an Agilent (model N5225A) vector network analyser. The complex permittivity and complex permeability parameters were measured with this setup from 8.2 GHz to 12.4 GHz: complex permeability $\mu_r = \mu' - j\mu''$ where μ', μ'' are permeability and magnetic loss, respectively, and complex permittivity $\varepsilon_r = \varepsilon' - j\varepsilon''$, where ε' and ε'' account for dielectric constant and dielectric loss, respectively. The analyzer was calibrated in air for accurate measurements.

X-RAY DIFFRACTION

The phase formation and crystallographic structure of $Ba_{0.5}Sr_{0.5}(CoIn)_xFe_{12-2x}O_{19}$ ferrite were examined at room temperature by XRD technique. The different curves obtained by XRD are displayed in Fig. 1. The observed diffraction patterns are in agreement with JCPDS card file number 51-1879 with lattice parameters $a = b = 5.8862$ (Å), $c = 23.137$ (Å) and cell volume $v = 694.24$ (Å^3), confirming the formation of hexagonal magnetoplumbite (M-type) crystal structure having space group P63/mmc. In Table I, lattice constants as well as cell volume increase with substitution, attributable to the large ionic radii of Co^{+2} (0.72 Å) and In^{+3} (0.91 Å) than Fe^{3+} (0.64 Å).[14,15] The 'c/a' ratio varies from 3.920 to 3.940 which is in agreement with a standard ratio of 3.9 and hence the M-type hexagonal structure is confirmed.[16]

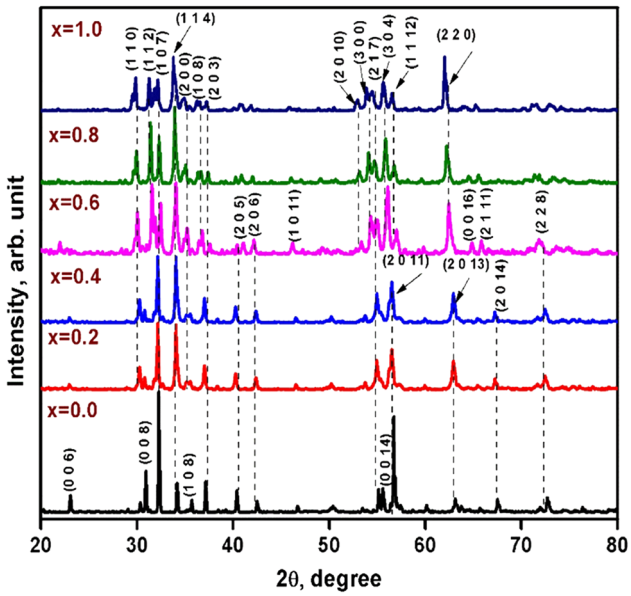

Fig. 1. X-ray diffraction patterns of $Ba_{0.5}Sr_{0.5}Co_xIn_xFe_{12-2x}O_{19}$ ferrite.

Table I. Lattice parameters of $Ba_{0.5}Sr_{0.5}Co_xIn_xFe_{12-2x}O_{19}$ ferrite

x	a (Å)	c (Å)	c/a	Cell volume (Å^3)
0.0	5.885	23.137	3.9315	693.9539
0.2	5.895	23.169	3.9302	697.2773
0.4	5.913	23.229	3.9284	703.3588
0.6	5.916	23.283	3.9355	705.7094
0.8	5.932	23.308	3.9291	710.2936
1.0	5.952	23.332	3.9200	715.8276

COMPLEX PERMITTIVITY AND COMPLEX PERMEABILITY

Figures 2 and 3 exhibit the change in electromagnetic parameters ε', ε'', μ' and μ'' in the frequency domain for different substitutions. The oscillations are seen in ε' and ε'' in the frequency regime and are governed by dipole polarization along with relaxation.[17] Co^{2+} and In^{3+} ions cause the non-monotonic variation of ε' and ε'' in compositions. Among substituted compositions, ε' increases from

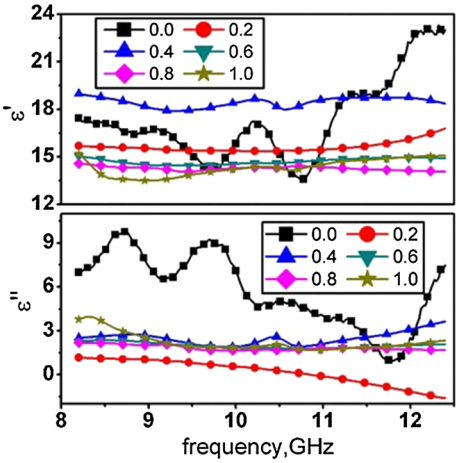

Fig. 2. Frequency dependence of ε' and ε'' in $Ba_{0.5}Sr_{0.5}Co_xIn_xFe_{12-2x}O_{19}$ hexaferrites.

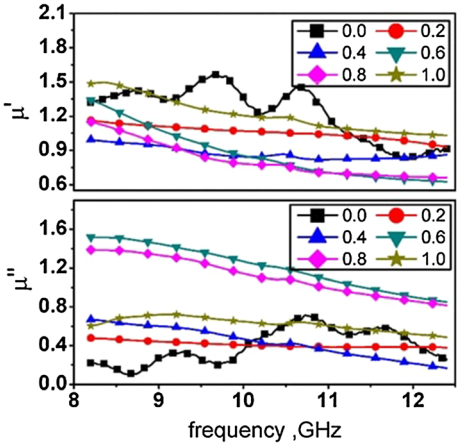

Fig. 3. Frequency dependence of μ' and μ'' in $Ba_{0.5}Sr_{0.5}Co_xIn_xFe_{12-2x}O_{19}$ hexaferrites.

composition $x = 0.2$ to $x = 0.4$ while further substitution causes its diminution thereafter. There is an increase in ε'' among substituted compositions, and $x = 0.6$, 0.8 have nearly the same values along with the investigated frequency regime. Both composition $x = 0.6$ and 1.0 exhibit nearly frequency-independent behaviour in ε' and ε''. Among the compositions, ε' in composition $x = 0.4$ occupies the maximum value in the examined frequency range from 8.2 GHz to 11.3 GHz, while non-substituted composition $x = 0.0$ has the maximum ε' in rest of the frequency region.

Permeability (μ') is maximum in composition $x = 0.0$ in the middle of the frequency regime, whereas it is maximum in $x = 1.0$ in the rest of the frequency regime. Compositions $x = 0.6$ and 0.8 have almost the same values in the high-frequency region. Both μ' and μ'' increase non-linearly among the substituted compositions, and more dispersion is noted in $x = 0.6$ and 0.8 compositions. Composition $x = 0.2$ displays frequency-independent behaviour in μ''.

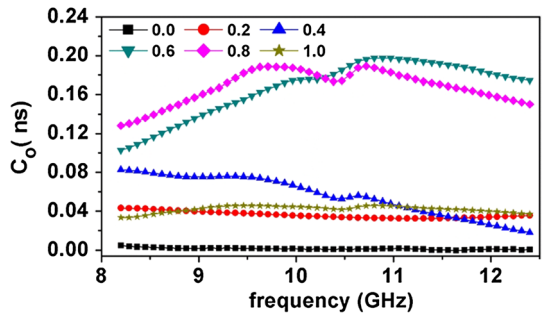

Fig. 4. Variation of C_o with frequency in $Ba_{0.5}Sr_{0.5}Co_xIn_xFe_{12-2x}O_{19}$ hexaferrites.

Considering the complex permittivity of the prepared $Ba_{0.5}Sr_{0.5}Co_xIn_xFe_{12-2x}O_{19}$ hexaferrite in the x-band, we can say that the dielectric constant and loss present the fluctuations with the former increasing with frequency for unsubstituted composition $x = 0.0$. This behaviour is probably associated with the fact that the dielectric constant and loss are primarily affected by exchange effects between Fe^{3+} and Fe^{2+} ions due to the ionic and electronic polarization which acts in the high-frequency region. In the present study, the substitution of Co^{2+} and In^{3+} in the hexaferrite reduces the Fe^{3+} ions depleting the exchange effect. Thus, substitution leads to stabilization in the value of the complex permittivity, as evident from Fig. 2. The complex permeability also incurs a similar effect with the reduction in exchange coupling between Fe^{3+} and Fe^{2+} due to the substitution, and relatively stable values are observed in substituted compositions in the investigated frequency region (Fig. 3), which is certainly an important result.

EDDY CURRENT

To explore the effect of eddy current in microwave attenuation, the following relation can be used:[17]

$$(\mu'')(\mu')^{-2}f^{-1} = 2\Pi\mu_0\sigma d^2 \qquad (1)$$

Let $C_o = (\mu'')(\mu')^{-2}f^{-1}$where d, μ_0 and σ are the thickness of composition, the permeability of vacuum, and the conductivity respectively.

From Fig. 4, it can be attributed that C_o follows almost constant value in $x = 0.0$, 0.2 and 1.0, while oscillations are seen in $x = 0.4$, 0.6 and 0.8. Thus, eddy current can attenuate microwave signals in $x = 0.0$, 0.2 and 1.0.

QUARTER-WAVELENGTH MECHANISM

This mechanism relates to the thickness of composition with wavelength and electromagnetic properties by following expression:[18]

$$t = \frac{n\lambda}{4} = \frac{n \cdot c}{4f\sqrt{|\mu_r \cdot \varepsilon_r|}} \qquad (2)$$

where n is an integer with values 1, 2, 3,..., t and accounts for the matching thickness, c is associated with the velocity of light and f is the matching frequency.

The transmission line theory explains microwave absorption in terms of reflection loss (RL) and input impedance (Z_{in}) with the following relation:

$$RL = 20\log\left|\frac{(Z_{in} - Z_o)}{(Z_{in} + Z_o)}\right| \quad (3)$$

where Z_o = 377 Ω is associated with the characteristic impedance of free space and Z_{in} relates the input impedance of a metal-backed material absorber which can be written as:[19]

$$Z_{in} = Z_o\sqrt{\frac{\mu_r}{\varepsilon_r}}\tanh\left[j\left(\frac{2\pi ft}{c}\right)\sqrt{(\mu_r \cdot \varepsilon_r)}\right] \quad (4)$$

The microwave absorption changes in direct proportion with RL; the more the RL, the larger will be the electromagnetic absorption. The large RL gives more microwave absorption.

The impedance matching criterion relates Z_{in} in equivalence with Z_o; i.e. $Z_{in} = Z_o$ for the perfect absorber.

In Figs. 5–8, microwave or electromagnetic absorption is studied by drawing the plots of the RL with respect to the frequency domain with varying simulated thickness. As the thickness is increased, RL peaks in composition x = 0.0, 0.2, 0.4 and 1.0 move into the low-frequency regime and vice versa. The mechanism of quarter-wavelength condition (Eq. 2) is attributed to this reciprocal trend between frequency and composition thickness. The maximal RL is −39.99 dB in composition x = 0.2 at 11.14 GHz and 1.6 mm. However, RL in x = 0.6 and 0.8 is less than −10 dB required for absorption.

To ascertain the relation between observed RL peaks in the compositions and quarter-wavelength mechanism, Eq. 2 is utilized to find out the calculated thickness (t_{cal}), and then a comparison is done with the simulated thickness (t_{sim}) used to find RL in Eq. 3. Figures 5–8 depict thickness (t) versus frequency plots: t_{cal} curves are plotted with n = 1 in Eq. 2. Evidently, composition x = 0.2 (Fig. 6) governs the quarter-wavelength mechanism since its t_{cal} is in conformity with t_{sim}, and, similarly, compositions x = 0.0, 0.4 and 1.0 also follow this mechanism for their observed RL peak (Figs. 5, 7, 8).

In composition x = 0.0, the height of RL dips increases non-systematically from 4.3 mm to 5.0 mm, and dips become broad with the increase in thickness. For composition x = 0.2, RL dips follows an increase in height from 1.5 mm to 1.6 mm and decrease subsequently with the further increase in thickness from 1.6 mm to 2.1 mm. For composition x = 0.4, the height of dips decreases with the thickness increment from 1.5 mm to 1.7 mm, while the height of dips increases with

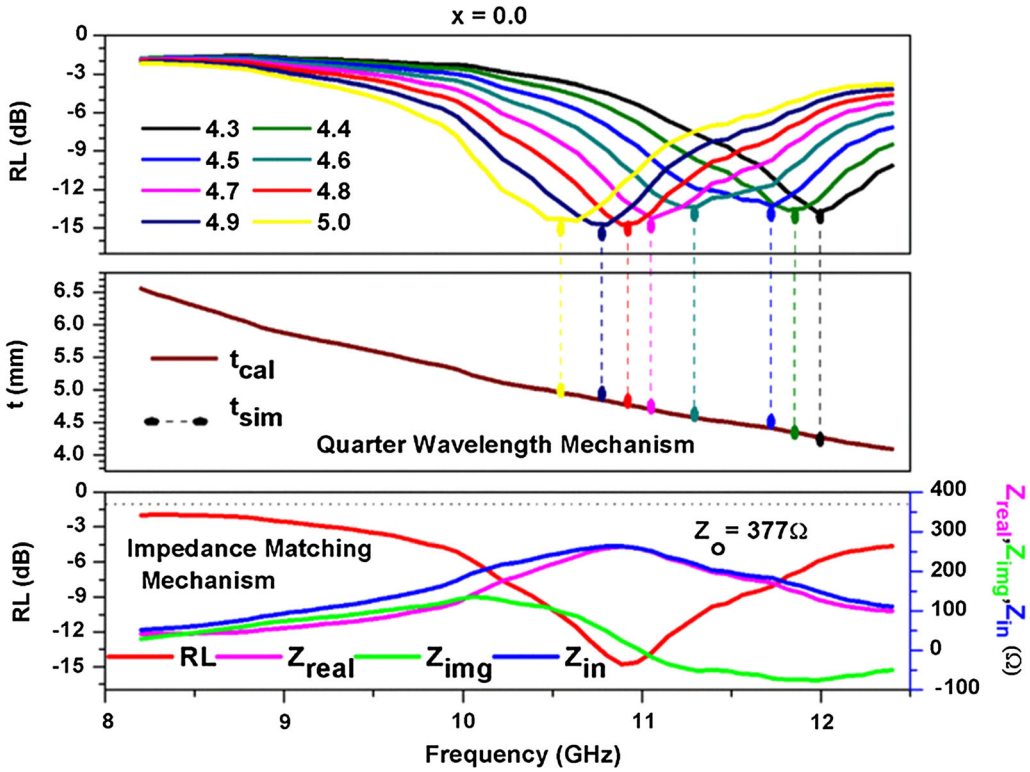

Fig. 5. Dependence of RL on Z_{real}, Z_{img}, Z_{in} and frequency for different thickness in composition x = 0.0.

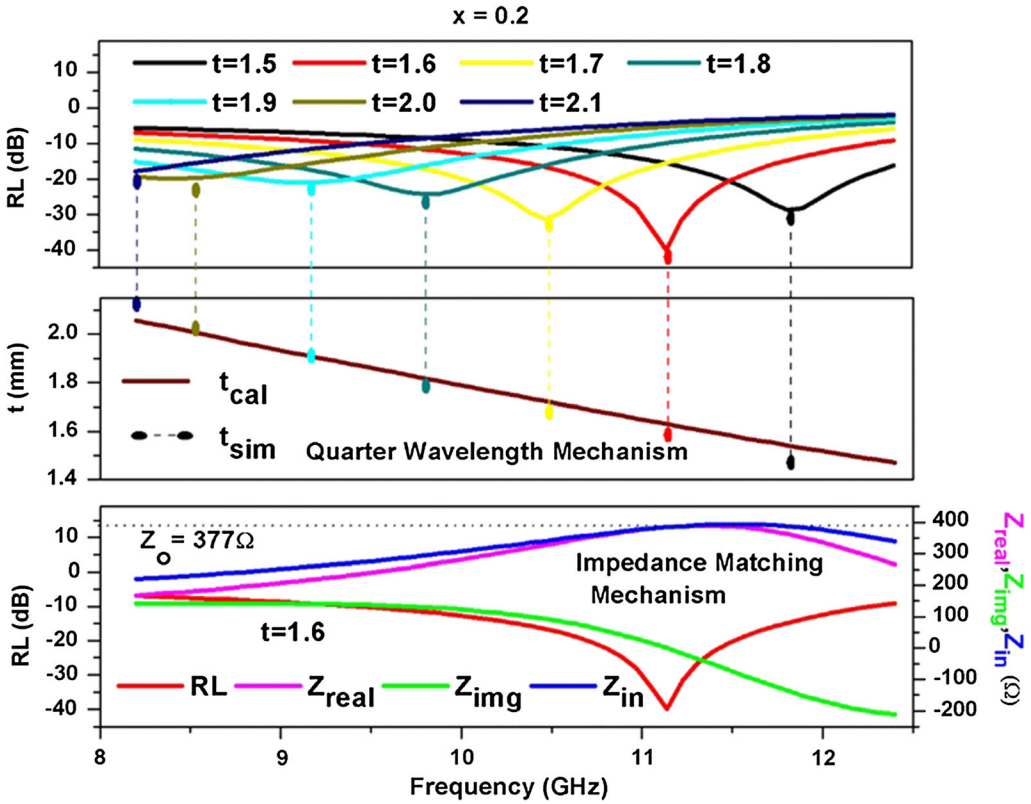

Fig. 6. Dependence of RL on Z_{real}, Z_{img}, Z_{in} and frequency for different thickness in composition $x = 0.2$.

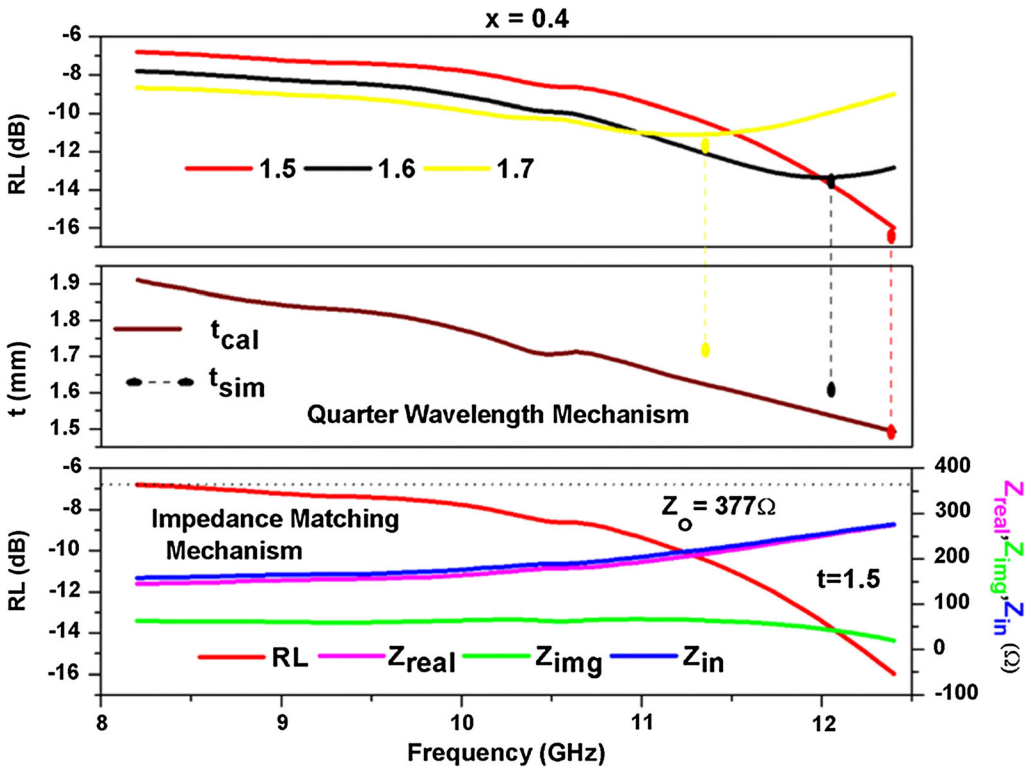

Fig. 7. Dependence of RL on Z_{real}, Z_{img}, Z_{in} and frequency for different thickness in composition $x = 0.4$.

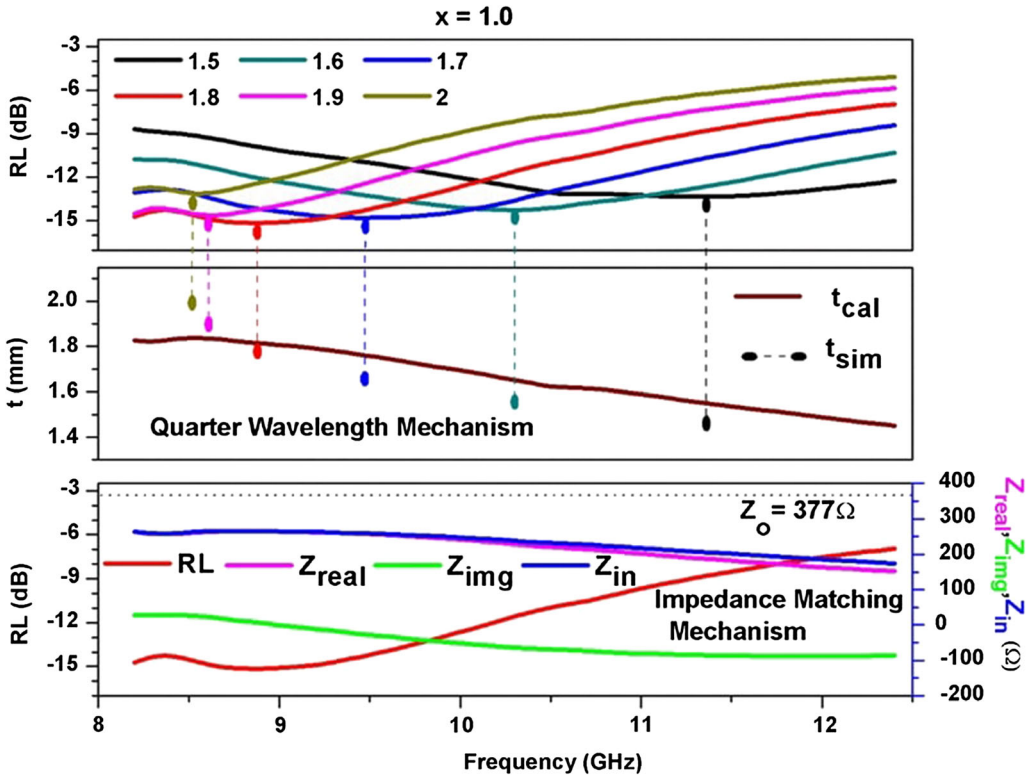

Fig. 8. Dependence of RL on Z_{real}, Z_{img}, Z_{in} and frequency for different thickness in composition x = 1.0.

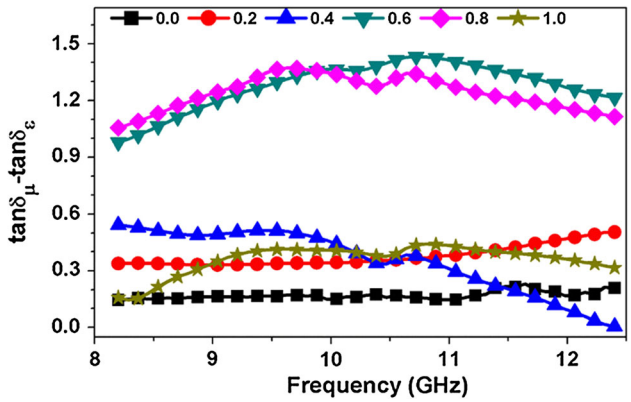

Fig. 9. Variation of minimum value of tan δ_ε – tan δ_μ versus frequency in compositions x = 0.0, 0.2, 0.4, 0.6, 0.8 and 1.0.

the increases in thickness from 1.5 mm to 1.8 mm in composition x = 1.0.

IMPEDANCE MATCHING

(i) *Loss Tangent*

The difference of tan δ_ε and tan δ_μ between accounts for impedance matching:[20] a small difference contributes to impedance matching and vice versa. Figure 9 shows the value of tan δ_ε – tan δ_μ in different compositions. It is clear that tan δ_ε – tan δ_μ is small in x = 0.0, 0.2, 0.4 and 1.0 as compared to x = 0.8 and 1.0, thus impedance matching is better in the former compositions. In x = 0.0, the difference is nearly the same from 8.2 GHz to 11 GHz, and a slight increment is found thereafter. In x = 0.2, the difference is almost the same from 8.2 GHz to 10 GHz and increases after that. The difference linearly decreases in x = 0.4 along the high-frequency region, while it is small in the low-frequency region in x = 1.0.

(ii) *Relation between impedance of material and free space*

The entire microwave signal will interact with material only if the impedance of the latter is equal to a characteristic impedance of free space. The details of this mechanism have been discussed elsewhere.[7] Thus, RL (Eq. 3) increases when Z_{real} and Z_{img} (Eq. 4) of material/absorber approach to 377 Ω and zero, respectively, and vice versa. In Figs. 6–9, the modulus of Z_{in}, Z_{real} and Z_{imag} are drawn to relate with the variation of RL at a given thickness of compositions. The drawn straight line in the plots is the characteristic impedance of free space; i.e. Z_o = 377 Ω. Some of the observed RL peaks follow this mechanism: for example, compositions x = 0.2 with 11.14 GHz and 1.6-mm thickness (Fig. 6).

Composition x = 0.2 has the maximum RL with Z_{img} near to zero and Z_{real} close to 377 Ω, and these parameters are better among all the compositions. Likewise, low RL is found in composition x = 0.6 and 0.8 with Z_{img} and Z_{real} more offset from zero and/or 377 Ω. Nonetheless, large magnetic loss μ'' is found in these compositions (Fig. 3). The impedance

mismatch, due to loss tangent (tan δ_ε – tan δ_μ), is also poor in compositions x = 0.6 and 0.8 as compared to compositions x = 0.0, 0.2, 0.4 and 1.0. Thus, maximum microwave/electromagnetic absorption (Fig. 6) seen in composition x = 0.2 is attributed to the impedance mechanism, quarter wavelength, eddy current and difference of tan δ_ε – tan δ_μ. Compositions x = 0.0, 0.4 and 1.0 have a small contribution of either of these factors for the observed low absorption.

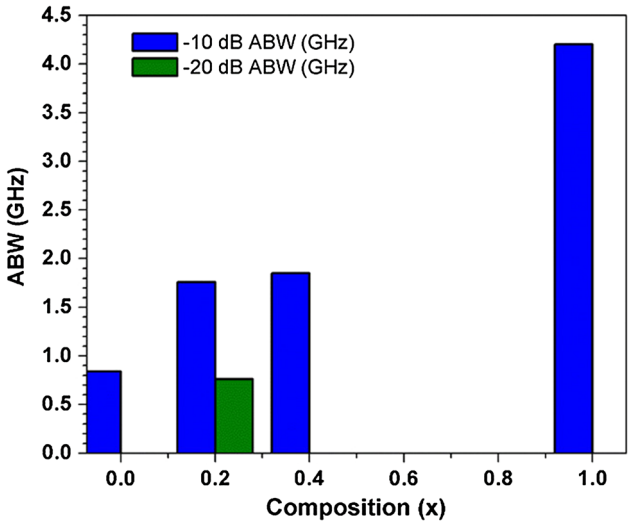

Fig. 10. Variation of maximum absorption bandwidth in compositions x = 0.0, 0.2, 0.4 and 1.0.

Figure 10 displays −10-dB and −20-dB bandwidth for the RL peaks of different compositions. It can be seen that −10-dB bandwidth is minimum (750 MHz) in composition x = 0.0, and a maximum value of 4.2 GHz occurs in substituted composition x = 1.0, covering the whole x-band spectrum. Only substituted composition x = 0.2 displays a −20-dB bandwidth of 0.76 GHz. Figure 11 the shows variation of maximum RL (RL_{max}) with the associated thickness in different compositions. There is a steep rise in RL_{max} with a lower substitution (x = 0.2), and gradual non-monotonic fall is observed thereafter from x = 0.2 to 1.0. The steep fall in thickness, associated with optimum RL, is also observed in substituted composition x = 0.2 with a value of 1.6 mm, and further substitution slightly increases the thickness.

CONCLUSIONS

M-type $Ba_{0.5}Sr_{0.5}Co_xIn_xFe_{12-2x}O_{19}$ hexagonal ferrites have been successfully prepared by the ceramic technique. The substitution of Co^{2+} and In^{3+} demonstrated superior electromagnetic absorption characteristics in the x = 0.2 composition along the majority of the examined x-band region. The absorption peaks tend to shift to the low-frequency regime with the increment in the thickness of compositions x = 0.0, 0.2, 0.4 and 1.0. Composition x = 1.0 encapsulates the complete x-band with an

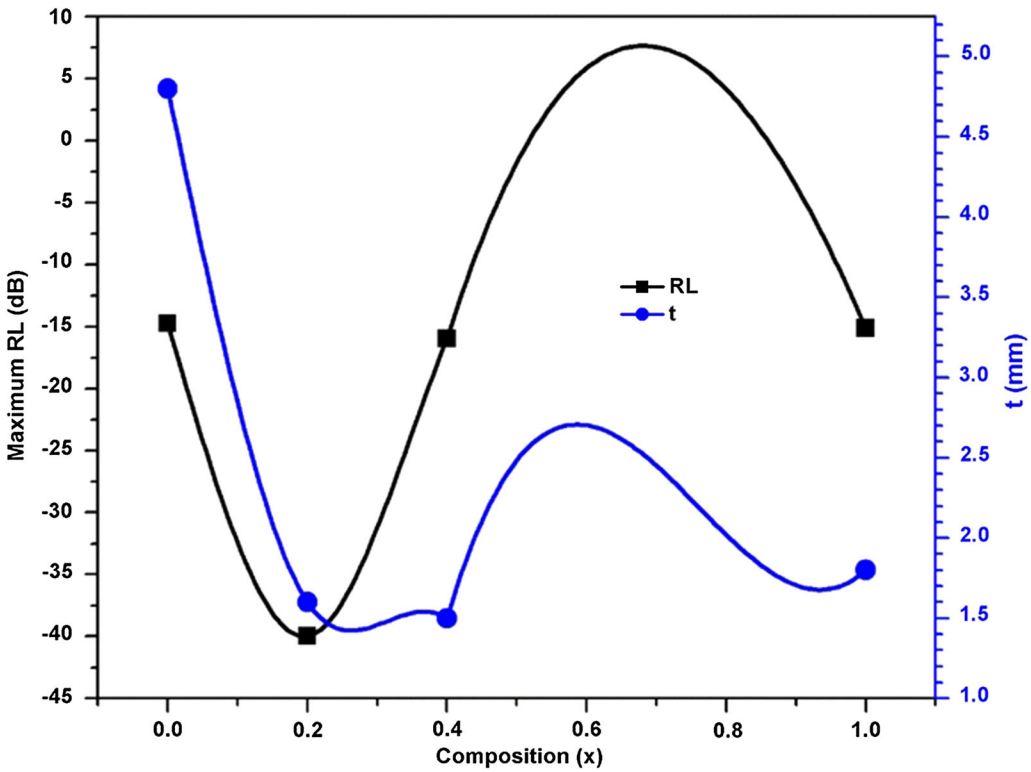

Fig. 11. Variation of maximum RL and thickness in compositions x = 0.0, 0.2, 0.4 and 1.0.

absorption bandwidth (−10 dB) of 4.2 GHz. The tailoring of absorption is possible by changing substitution, frequency and thickness. The investigated compositions have good potential for wide/narrowband absorber applications.

REFERENCES

1. R. Taherian, A. Soleymani, and S.A. Manafi, *IEEE Magn. Lett.* 7, 1 (2016).
2. C. Li, B. Wang, and J. Wang, *J. Magn. Magn. Mater.* 324, 1305 (2012).
3. M. Radwan, M.M. Rashad, and M.M. Hessien, *J. Mater. Process. Technol.* 181, 106 (2007).
4. D. Guo, P. Zhou, J. Hou, X. Luo, X. Wang, and L. Deng, *IEEE Trans. Magn.* 51, 1 (2015).
5. I.S. Unver and Z. Durmus, *IEEE Trans. Magn* 53, 1 (2017).
6. J. Singh, C. Singh, D. Kaur, S.B. Narang, R. Jotania, and R. Joshi, *J. Mater. Sci.-Mater. Electron.* 28, 2377 (2017).
7. J. Singh, C. Singh, D. Kaur, S.B. Narang, R. Joshi, S. Mishra, R. Jotania, M. Ghimire, and C.C. Chauhan, *Mater. Des.* 110, 749 (2016).
8. K.C.B. Naidu, S. RoopasKiran, and W. Madhuri, *IEEE Trans. Magn.* 53, 1 (2017).
9. I. Sadiq, S. Naseem, M.N. Ashiq, M.A. Iqbal, I. Ali, M.A. Khan, S. Niaz, and M.U. Rana, *J. Magn. Magn. Mater.* 395, 159 (2015).
10. K.-K. Ji, Y. Li, and M.-S. Cao, *J. Mater. Sci. Mater. Electron.* 27, 5128 (2016).
11. A.V. Trukhanov, S.V. Trukhanov, V.G. Kostishin, L.V. Panina, M.M. Salem, I.S. Kazakevich, V.A. Turchenko, V.V. Kochervinskii, and D.A. Krivchenya, *Phys. Solid State* 59, 737 (2017).
12. S.V. Trukhanov, A.V. Trukhanov, V.A. Turchenko, An V. Trukhanov, D.I. Tishkevich, E.L. Trukhanova, T.I. Zubar, D.V. Karpinsky, V.G. Kostishyn, L.V. Panina, D.A. Vinnik, S.A. Gudkova, E.A. Trofimov, P. Thakur, A. Thakur, and Y. Yang, *J. Magn. Magn. Mater.* 457, 83 (2018).
13. V.A. Turchenko, S.V. Trukhanov, A.M. Balagurov, V.G. Kostishyn, A.V. Trukhanov, L.V. Panina, and E.L. Trukhanova, *J. Magn. Magn. Mater.* 464, 139 (2018).
14. J. Singh, C. Singh, D. Kaur, S.B. Narang, R. Jotania, and R. Joshi, *J. Alloys Compd.* 695, 792 (2017).
15. R.K. Puri, M. Singh, and S.P. Sud, *J. Mater. Sci.* 29, 2182 (1994).
16. T.R. Wagner, *J. Solid State Chem.* 136, 120 (1998).
17. H. Lv, G. Ji, H. Zhang, M. Li, Z. Zuo, Y. Zhao, B. Zhang, D. Tang, and Y. Du, *Sci. Rep.* 5, 18249 (2015).
18. B. Wang, J. Wei, Y. Yang, T. Wang, and F. Li, *J. Magn. Magn. Mater.* 323, 1101 (2011).
19. T. Inui, K. Konishi, K. Oda, and E.E.E. Trans, *Magn.* 35, 3148 (1999).
20. G.M. Shi, Y.F. Li, L. Ai, and F.N. Shi, *J. Alloys Compd.* 680, 735 (2016).